arXiv:1401.7489v1 [astro-ph.SR] 29 Jan 2014

Physical Nature and Timing Variations of the Eclipsing System V407 Pegasi

Jae Woo Lee, Jang-Ho Park, Kyeongsoo Hong, Seung-Lee Kim, and Chung-Uk Lee

Korea Astronomy and Space Science Institute, Daejeon 305-348, Korea

jwlee@kasi.re.kr, pooh107162@kasi.re.kr, kshong@kasi.re.kr, slkim@kasi.re.kr, leecu@kasi.re.kr

ABSTRACT

New multiband CCD photometry is presented for V407 Peg; the R_C light curves are the first ever compiled. Our light curves, displaying a flat bottom at secondary minimum and an O'Connell effect, were simultaneously analyzed with the radial-velocity (RV) curves given by Rucinski et al. (2008). The light changes of the system are best modeled by using both a hot spot on the secondary star and a third light. The model represents historical light curves also. All available minimum epochs, including our six timing measurements, have been examined and indicate that the eclipse timing variation is mainly caused by light asymmetries due to the spot activity detected in the light-curve synthesis. The hot spot may be produced as a result of the impact of the gas stream from the primary star. Our light and velocity solutions indicate that V407 Peg is a totally-eclipsing A-type overcontact binary with values of q=0.251, i=87°.6, ΔT=496 K, f=61 %, and l_3=11∼16 %. Individual masses and radii of both components are determined to be M_1=1.72 $M_\odot$, M_2=0.43 $M_\odot$, R_1=2.15 $R_\odot$, and R_2=1.21 $R_\odot$. These results are very different from previous ones, which is probably caused by the light curves with distorted and inclined eclipses used in those other analyses. The facts that there are no objects optically related with the system and that the seasonal RVs show a large discrepancy in systemic velocity indicate that the third light source most likely arises from a tertiary component orbiting the eclipsing pair.

Subject headings: binaries: eclipsing — stars: fundamental parameters — stars: individual (V407 Pegasi) — stars: spots

1. INTRODUCTION

V407 Peg (BD + 14°5016, 2MASS J23365535+1548063, TYC 1720-658-1; V=+9.28; F0V) was discovered to be an eclipsing variable by the Semi-Automatic Variability Search program at the Piwnice Observatory in Poland (Maciejewski et al. 2002, MKN). The light curves in the BV bandpasses were typical of W UMa type and the maximum (Max II) following the secondary minimum was about 0.04 mag fainter than Max I. Maciejewski and collaborators (Maciejewski et

al. 2003; Maciejewski & Ligęza 2004) obtained double-line radial velocity (RV) curves with values of K_1=54.7 km s^{-1}, K_2=233.9 km s^{-1}, and γ=22.1 km s^{-1}. By combining the BV light curves of MKN with the spectroscopic solutions, they reported that V407 Peg is an A-type overcontact binary with parameters of i=72°.6, Δ $(T_1 - T_2)$=329 K, f=54%, M_1=1.48 $M_\odot$, and M_2=0.35 $M_\odot$. The light variations were explained by a hot spot located on the surface of the more massive primary star.

Since then, Rucinski et al. (2008) measured 63 precise RVs at the David Dunlap Observatory (DDO) and derived spectroscopic elements (K_1=63.9 km s^{-1}, K_2=250.0 km s^{-1}, and γ=9.1 km s^{-1}) and a spectral type of F0V. These differ from previous results; the discrepancy is thought to be partially caused by the older RV curves, which lack coverage continuity. Recently, Deb & Singh (2011) computed the binary parameters of V407 Peg using the spectroscopic solutions of Rucinski et al. (2008) and the V-band observations from the All Sky Automated Survey (ASAS) project (Pojmanski 1997, 2002). Their results indicate that this system is a partially eclipsing binary with i=71°.1, Δ $(T_1 - T_2)$=862 K, f=81%, M_1=1.92 $M_\odot$, and M_2=0.49 $M_\odot$. On the other hand, the orbital period of V407 Peg has been examined by Zasche (2011) only once. From the O–C display based on newly derived minima and on historical data, he showed that the system has displaced secondary minima and suggested that the phenomenon is probably caused by asymmetrical light curves. Both eclipses from the MKN and ASAS data were asymmetric and distorted, but did not vary significantly with time.

Although V407 Peg has been studied photometrically and spectroscopically, the published light curves were somewhat incomplete or have been spread over several seasons. Intrinsic light variations for the system due to starspots and a third light source have not yet been considered in detail. Additionally, the eclipse timing variations still have not been described as conclusively as can be desired. In this paper, we present new multiband light curves and measure the physical properties of the eclipsing system from detailed studies of all available data, such as light and RV curves, and eclipse timings.

2. CCD PHOTOMETRIC OBSERVATIONS

New photometry of V407 Peg was performed on 14 nights from 2011 September 21 through December 27 in order to obtain multiband light curves. The observations were conducted using a PIXIS: 2048B CCD camera and a BVR_C filter set attached to the 61-cm reflector at Sobaeksan Optical Astronomy Observatory (SOAO) in Korea. The instrument and reduction method are the same as those described by Lee et al. (2013). Since the image field-of-view (FOV) was large enough to observe a few tens of nearby stars simultaneously, we monitored them along with the program target. Following the procedure described by Lee et al. (2010), potentially useful field stars were examined in detail for any peculiar light variations. Then, two non-variable candidates (TYC 1720-880-1 and TYC 1720-986-1) were combined using a weighted average to make an artificial reference star that would be optimal for our photometry.

A total of 4636 individual observations was obtained in the three bandpasses (1531 in B, 1568 in V, and 1537 in $R_{\rm C}$) and a sample of those observations is provided in Table 1. The light curves of V407 Peg are plotted in Figure 1 as differential magnitudes between the variable and artificial comparison stars *versus* orbital phases; these data were computed according to the ephemeris for our hot-spot model on the less massive secondary star described in the following section. As shown in the figure, the SOAO observations are evenly distributed in phase and display the wavelength-dependent O'Connell effect for all bandpasses.

3. LIGHT AND VELOCITY SOLUTIONS

Our observations are typical of a short-period overcontact binary and display a flat bottom at secondary minimum, indicating that V407 Peg belongs to the A-type of W UMa stars. Further, as do the light curves of MKN and ASAS, the SOAO data are asymmetrical and Max I is brighter than Max II by about 0.074, 0.056, and 0.042 mag for the B, V, and $R_{\rm C}$ bandpasses, respectively. The light maxima (Max I and Max II) are displaced to around phases 0.238 and 0.755, respectively, and the primary minima are distorted and inclined, which may be caused by local photospheric inhomogeneities. In principle, these might be due to spot activity caused either by a magnetic dynamo or by impact from mass transfer between the components.

In order to obtain a unique set of the binary parameters for V407 Peg, our light curves were simultaneously modeled with the RV curves of Rucinski et al. (2008), taking into account proximity effects. We used contact mode 3 of the Wilson-Devinney synthesis code (Wilson & Devinney 1971, WD) and a weighting scheme similar to that for the eclipsing systems RU UMi (Lee et al. 2008) and WZ Cyg (Lee et al. 2011). Table 2 lists the radial velocity and light-curve sets of the binary system simultaneously analyzed in this paper and their standard deviations (σ). The effective temperature of the larger and hotter primary star was assumed to be T_1=6980 K, according to its spectral type F0V given by Rucinski et al. (2008). The gravity-darkening exponents and the bolometric albedos were fixed at standard values of g=0.32 and A=0.5 for stars with common convective envelopes. The logarithmic bolometric (X, Y) and monochromatic (x, y) limb-darkening coefficients were interpolated from the values of van Hamme (1993) and were used in concert with the model atmosphere option. Also, a synchronous rotation for both components and a circular orbit were adopted. In this paper, the subscripts 1 and 2 refer to the primary and secondary stars being eclipsed at Min I (at phase 0.0) and Min II, respectively.

Our analyses were carried out through three stages. In the first stage, the RV and light curves in Table 2 were solved, permitting no perturbations such as starspots or third light (l_3). The results are plotted as the short-dashed curves in Figure 1, for which the model light curves do not fit well the eclipse minima as well as light level at the first quadrature. In the second stage, the SOAO light curves were reanalyzed with the RV data by using the unperturbed solutions as the initial values and then considering a spot on either of the components. But, even the spotted solutions displayed as the long dashes in the same figure indicate that the observed eclipses are

shallower than the computed ones and that the differences of the eclipse depths could be dependent on bandpasses. The fact may suggest a third light source in the system. Lastly, we modeled the observations including both spot and third light perturbations. Final results are given in Table 3, in which Model 1 and Model 2 represent the hot-spot model on the primary and secondary stars, respectively. Although it is not easy to discriminate between the two, we can see that Model 2 gives lightly smaller values for the sum of the residuals squared ($\Sigma W(O-C)^2$) than does Model 1. The synthetic light curves from Model 2 are plotted as the solid curves in Figure 1, while the synthetic RV curves are plotted in Figure 2 together with the measurements of Maciejewski & Ligęza (2004) and Rucinski et al. (2008). As can be seen in the figures, our hot-spot model describes the SOAO multiband data quite well. Separate trials for a cool spot on either of the components were not so successful as the trials for the hot-spot models. In all the procedures that have been described, we included an orbital eccentricity as a free parameter but found that the parameter retained a value of zero, which was within its margin of error.

To study the spot behavior of V407 Peg further and to examine whether our solutions can reasonably describe the historical light curves, we analyzed the MKN and ASAS data by adjusting only the orbital ephemeris (T_0 and P), spot, and luminosity among the Model 2 parameters. These results appear in Table 4 and are plotted in Figure 3 as the continuous curves. From the analyses, we can conclude that the hot-spot model on the secondary star satisfies all curves of V407 Peg quite well and gives a good representation of the binary system for both the photospheric and spot descriptions. As listed in Tables 3–4, the spot parameters have been almost constant with time since the discovery of the eclipsing pair and the stellar light ratios have not changed appreciably as a result of the spot modeling. Moreover, because V407 Peg should not have a deep common convective envelope as surmised from its spectral type and temperatures, the hot spot may be produced by stable mass transfer between the binary components.

4. ECLIPSE TIMING VARIATIONS

From the SOAO observations, eclipse timings and their errors for each filter were determined using the method of Kwee & van Woerden (1956, KvW). Six new weighted times of minimum light are listed in the first column of Table 5, wherein two of the times (HJD 2,452,552.4416 and 2,452,582.3735) were derived by us from the individual measurements of MKN. In addition to these, 52 CCD timings have been collected from the literature (Maciejewski et al. 2002; Brát et al. 2011; Zasche 2011; Liakos & Niarchos 2011; Gokay et al. 2012; Diethelm 2012, 2013, Gürsoytrak et al. 2013).

For ephemeris computations, weights for the eclipse timings were scaled as the inverse squares of their errors. In order to obtain a mean light ephemeris and to form an eclipse timing diagram, we applied a linear least-squares fit to all times of minimum light of V407 Peg and thus found an

improved ephemeris, as follows:

$$C = \text{HJD } 2452533.97494(21) + 0.636883596(47)E, \quad (1)$$

where the parenthesized numbers are the 1σ-error values for the last digit of each term of the ephemeris. The resulting O–C residuals calculated with equation (1) are plotted in Figure 4, in which the filled and open circles are the primary (Min I) and secondary (Min II) minima, respectively, from the literature. The up triangles represent the minimum times obtained using the KvW method from the MKN and SOAO data.

As displayed in Figure 4, the O–C residuals from both eclipses are not in phase with each other and then this discrepancy can be attributed to the rotation of the apsidal line of the eccentric orbit due to tidal forces between the binary components. For apsidal motion, the O–C residuals for primary minima are nearly 180° out of phase with those for the secondary. However, because the light-curve synthesis of V407 Peg indicates that the binary orbit is circular, the apsidal motion cannot explain the timing variations. Zasche (2011) suggested that the displaced secondary minima are caused by asymmetry of the light curves, resulting from a gas stream impact between the two components. In W UMa binaries, times of minimum light are shifted from the real conjunctions by asymmetrical eclipse minima due to stellar activity such as starspots (Kalimeris et al. 2002) and/or even by the method of measuring the eclipse timing (Maceroni & van't Veer 1994). The light-curves synthesis method developed by WD is capable of extracting the conjunction instants and gives more and better information than that of the other methods, which do not consider spot activity and are based on observations during minimum alone. In reality, Lee et al. (2009) showed that the minimum epochs of the overcontact binary AR Boo have been systematically shifted by light asymmetries due to spot activity.

In order to check for this possibility, we calculated the timings for each of all available eclipses using the WD code. The results are listed in the second column of Table 5 and are illustrated with the down triangles in Figure 4. As shown in the third column of this table, there are systematic runs of differences between the KvW timings and the WD ones, which are negative for Min I and positive for Min II. These differences are caused by a hot spot on the secondary component presented to the observer after Min I and before Min II. In Figure 4, we can see that the eclipse timing variations are mainly caused by the presence of a large hot spot which produces the asymmetrical light curves of V407 Peg.

5. DISCUSSION AND CONCLUSIONS

New multiband CCD light curves display complete eclipses leading to well-determined system parameters. Our light and velocity solutions indicate that V407 Peg is a totally-eclipsing A-type overcontact binary with a fill-out factor of about 60 % and with a temperature difference of 496 K between the components. The binary model with a third light and a single hot spot on the less massive secondary component fits all available light curves quite well. We think that the hot

spot may be produced as a result of the impact of the gas stream from the primary star, which is a dominant cause of the eclipse timing variations. The third light of 11∼16 % in all bandpasses could come from a tertiary object either gravitationally bound to or only optically related with the eclipsing pair. We do not see such an object optically resolved on our time-series CCD images. Although the third light source was not detected in the spectrograms of Rucinski et al. (2008), the two datasets of Maciejewski & Ligęza (2004) and Rucinski et al. (2008), taken at the DDO and processed using the broadening function algorithm (Rucinski 2002), show a large discrepancy of about 13 km s^{-1} in systemic velocity (γ). If the velocity difference is real, the third light most likely arises from the existence of a third component orbiting the eclipsing binary, which is a member of a triple system (Pribulla & Rucinski 2006).

The simultaneous analysis of light and RV curves allowed us to compute the absolute parameters given in Table 6, together with those of Deb & Singh (2011) for comparison. The luminosity (L) and bolometric magnitudes ($M_{\rm bol}$) were obtained by adopting $T_{\rm eff\odot}$=5,780 K and $M_{\rm bol\odot}$=+4.73 for solar values. In accordance with the unreliability in spectral classification, it was assumed that the temperature of each component had an error of 200 K. The bolometric corrections (BCs) were obtained from the relation between $\log T_{\rm eff}$ and BC given by Torres (2010). With an apparent visual magnitude of V=+9.28 at maximum light, our computed light ratio, and the interstellar absorption of $A_{\rm V}$=0.186 (Schlafly & Finkbeiner 2011), we determined the distance to the system to be 280±21 pc. The absolute parameters presented in this paper differ much from those of Deb & Singh (2011). Considering our orbital inclination to be about 16 deg larger than that of earlier studies, the discrepancy is probably caused the ASAS light curves' displaying of inclined, partial eclipses.

From our absolute parameters, it is possible to consider the evolutionary state of V407 Peg in terms of mass-radius, mass-luminosity, and the Hertzsprung-Russell (HR) diagrams. The locations of the component stars in these diagrams are shown in Figure 5, together with those of other well-studied overcontact binaries. The data are taken from the compilations of Yakut & Eggleton (2005), Li et al. (2008), and Christopoulou et al. (2012). As can be seen in the figure, the binary components do conform to the general pattern of W UMa systems. The primary star lies in the main-sequence band, while the secondary is oversized and overluminous for its mass. This could be explained as a result of energy transfer from the more massive primary toward the less massive secondary star (e.g., Hilditch et al. 1988; Li et al. 2008). Because the light-curve synthesis of the system indicates that mass is moving between both components, a secular period variation may be produced through the mass transfer in the system. More systematic and continuous high-resolution observations (photometry and spectroscopy) will help to identify and understand the orbital period variation of V407 Peg.

We would like to thank the staff of the Sobaeksan Optical Astronomy Observatory for assistance during our observations. This research has made use of the Simbad database maintained at CDS, Strasbourg, France. This work was supported by the KASI (Korea Astronomy and Space Science

Institute) grant 2014-1-400-06.

REFERENCES

Brát, L., et al. 2011, Open Eur. J. Var. Stars, 137, 1

Christopoulou, P.-E., Papageorgiou, A., Vasileiadis, T., & Tsantilas, S. 2012, AJ, 144, 149

Deb, S., & Singh, H. P. 2011, MNRAS, 412, 1787

Diethelm, R. 2012, Inf. Bull. Variable Stars, 6011, 1

Diethelm, R. 2013, Inf. Bull. Variable Stars, 6042, 1

Gokay, G., et al. 2012, Inf. Bull. Variable Stars, 6039, 1

Gürsoytrak, H., et al. 2013, Inf. Bull. Variable Stars, 6075, 1

Hilditch, R. W., King, D. J., & McFarlane, T. M. 1988, MNRAS, 231, 341

Kalimeris, A., Rovithis-Livaniou, H., & Rovithis, P. 2002, A&A, 387, 969

Kwee, K. K., & van Woerden, H. 1956, Bull. Astron. Inst. Netherlands, 12, 327

Lee, J. W., Kim, C.-H., Kim, S.-L., Lee, C.-U., Han, W., & Koch, R. H. 2008, PASP, 120, 720

Lee, J. W., Youn, J.-H., Lee, C.-U., Kim, S.-L., & Koch, R. H. 2009, AJ, 138, 478

Lee, J. W., et al. 2010, AJ, 139, 898

Lee, J. W., Kim, S.-L., Lee, C.-U., Kim, H.-I., Park, J.-H., & Hinse, T. C. 2011, AJ, 142, 12

Lee, J. W., Hinse, T. C., & Park, J.-H. 2013, AJ, 145, 100

Li, L., Zhang, F. Han, Z., Jiang, D., & Jiang, T. 2008, MNRAS, 387, 97

Liakos, A., & Niarchos, P. 2011, Inf. Bull. Variable Stars, 6005, 1

Maceroni, C., & van't Veer, F. 1994, A&A, 289, 871

Maciejewski, G., Karska, A., & Niedzielski, A. 2002, Inf. Bull. Variable Stars, 5343, 1 (MKN)

Maciejewski, G., Ligęza, P., & Karska, A. 2003, Inf. Bull. Variable Stars, 5400, 1

Maciejewski, G., & Ligęza, P. 2004, Inf. Bull. Variable Stars, 5504, 1

Pojmanski, G. 1997, Acta Astron., 47, 467

Pojmanski, G. 2002, Acta Astron., 52, 397

Pribulla, T., & Rucinski, S. M. 2006, AJ, 131, 2986

Rucinski, S. M. 2002, AJ, 124, 1746

Rucinski, S. M., et al. 2008, AJ, 136, 586

Schlafly, E. F., & Finkbeiner, D. P. 2011, AJ, 737, 103

Torres, G. 2010, AJ, 140, 1158

Tout, C. A., Pols, O. R., Eggleton, P. P., & Han, Z. 1996, MNRAS, 281, 257

Wilson, R. E., & Devinney, E. J. 1971, ApJ, 166, 605

Yakut, K., & Eggleton, P. P. 2005, ApJ, 629, 1055

Van Hamme, W. 1993, AJ, 106, 209

Zasche, P. 2011, Inf. Bull. Variable Stars, 5991, 1

This preprint was prepared with the AAS LaTeX macros v5.2.

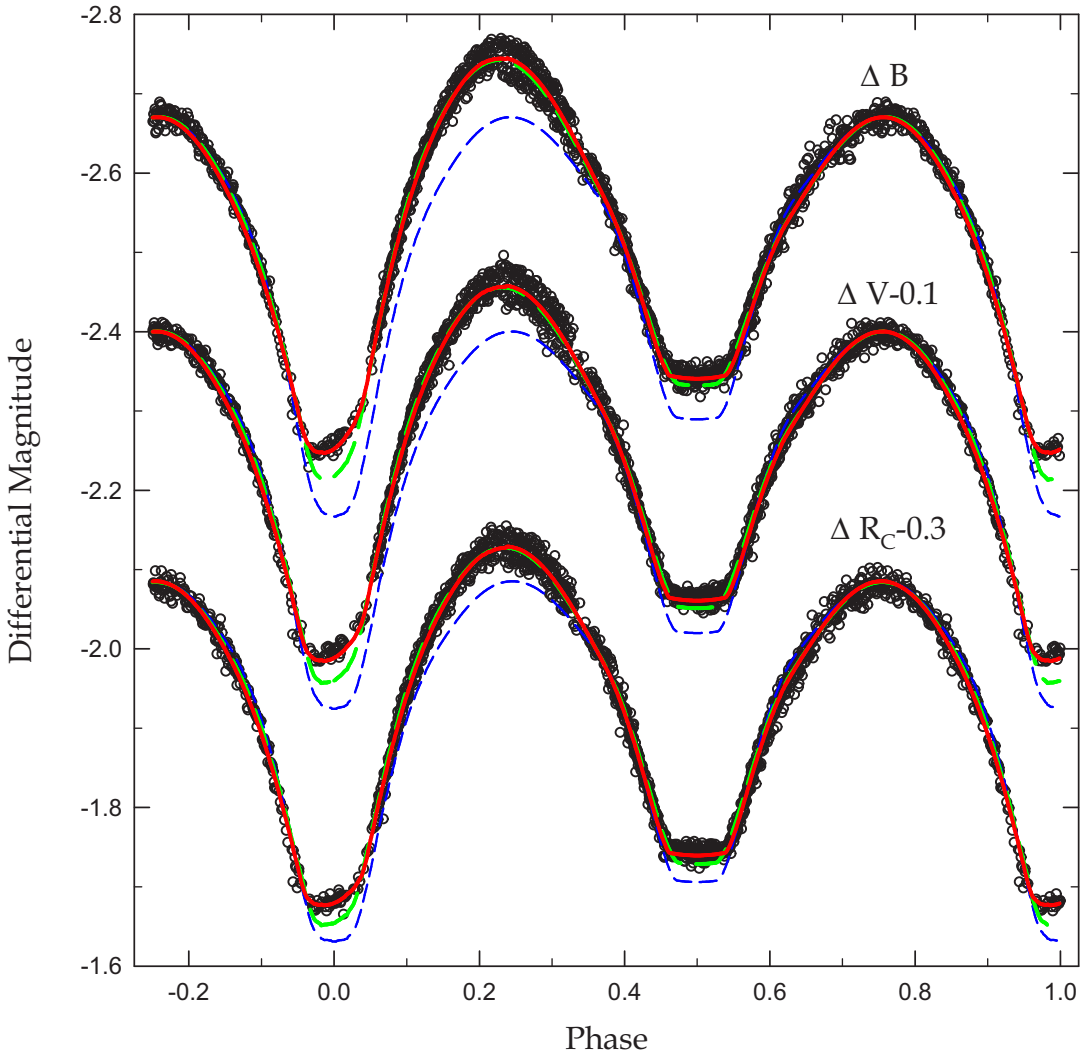

Fig. 1.— $BVR_{\rm C}$ observations of V407 Peg with fitted model light curves. The short and long dashes are computed without and with a spot, respectively, and the solids represent the solutions obtained with both a spot and a third light (l_3). See the text for details.

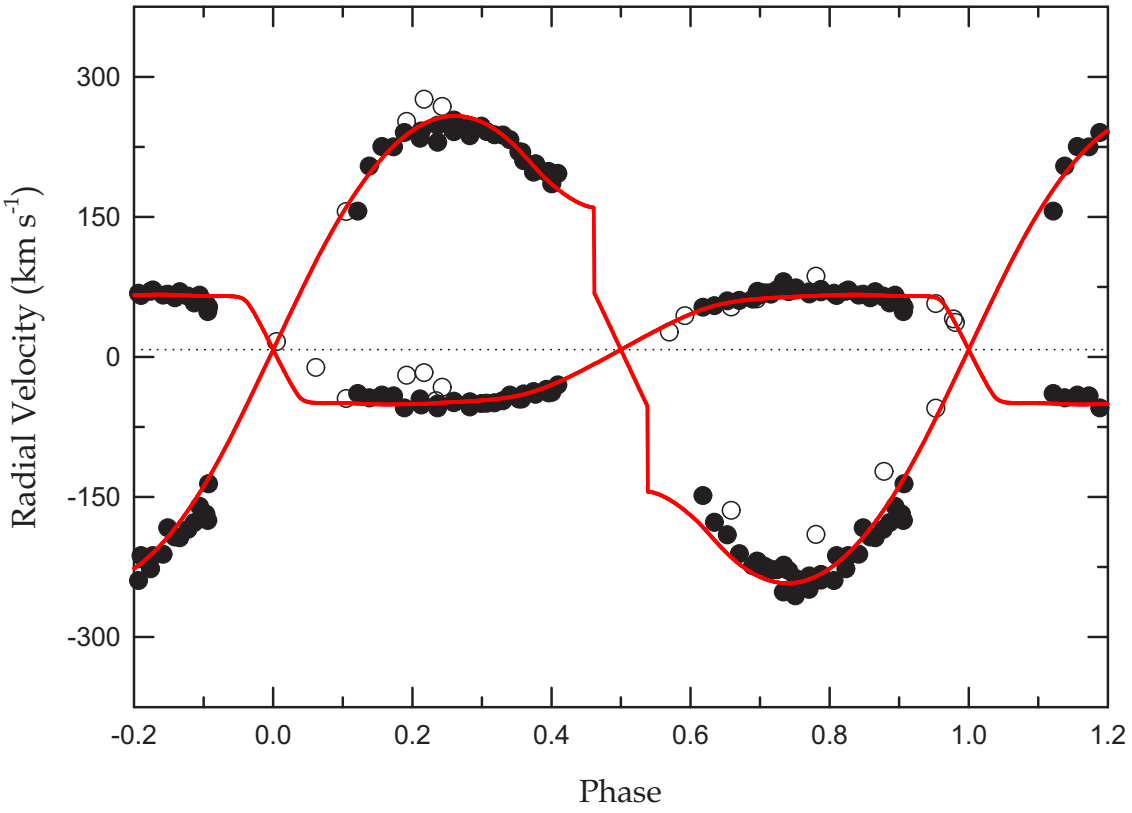

Fig. 2.— Radial-velocity curves of V407 Peg. The open and filled circles are the measures of Maciejewski & Ligęza (2004) and Rucinski et al. (2008), respectively, while the solid curves denote the results from consistent light and RV curve analysis. The dotted line refers to the system velocity of 7.9 km s^{-1}.

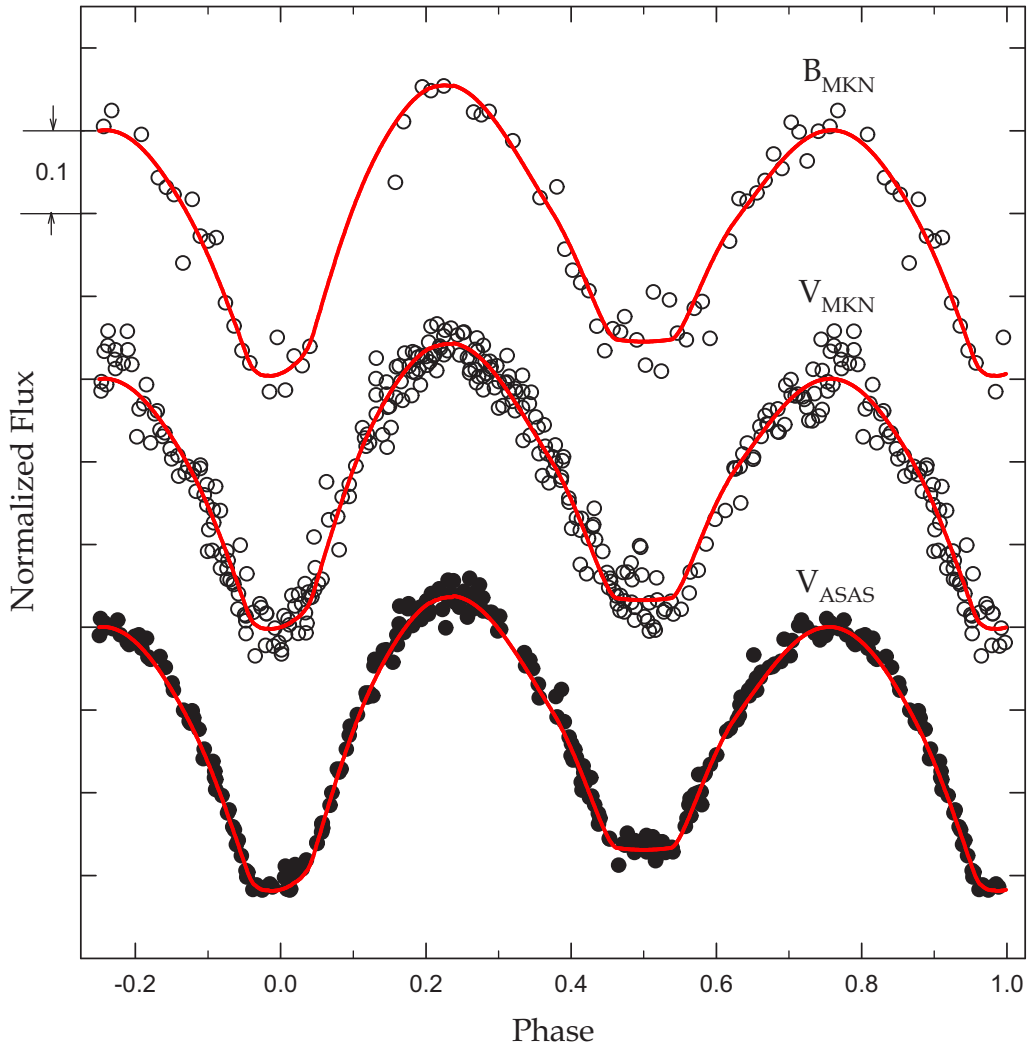

Fig. 3.— Historical light curves of V407 Peg. The open and filled circles are the measures of MKN and ASAS, respectively. The continuous curves represent solutions obtained with the spot-model parameters listed in Table 4.

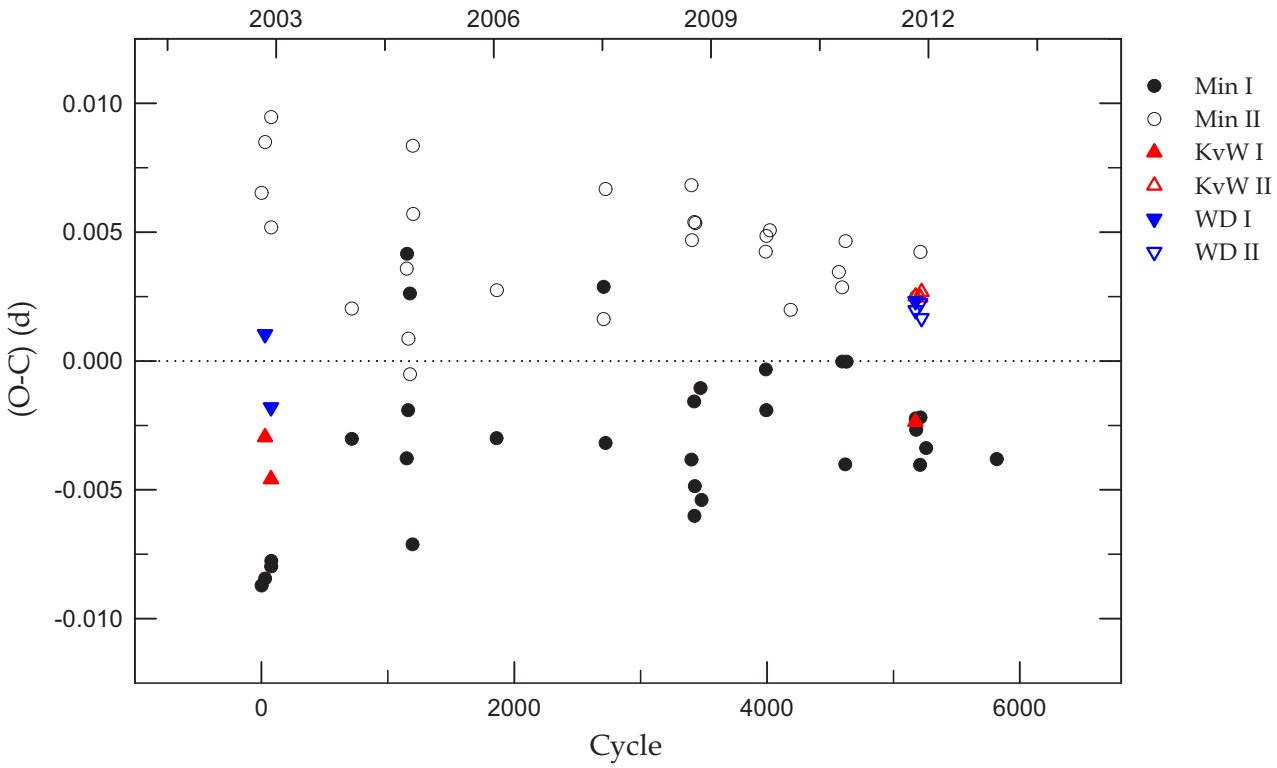

Fig. 4.— *O–C* diagram of V407 Peg. The filled and open circles are the primary (Min I) and secondary (Min II) minima, respectively, from the literature. The triangle symbols represent the minimum times in Table 5, obtained by us from the MKN and SOAO data using the KvW method and the WD synthesis code.

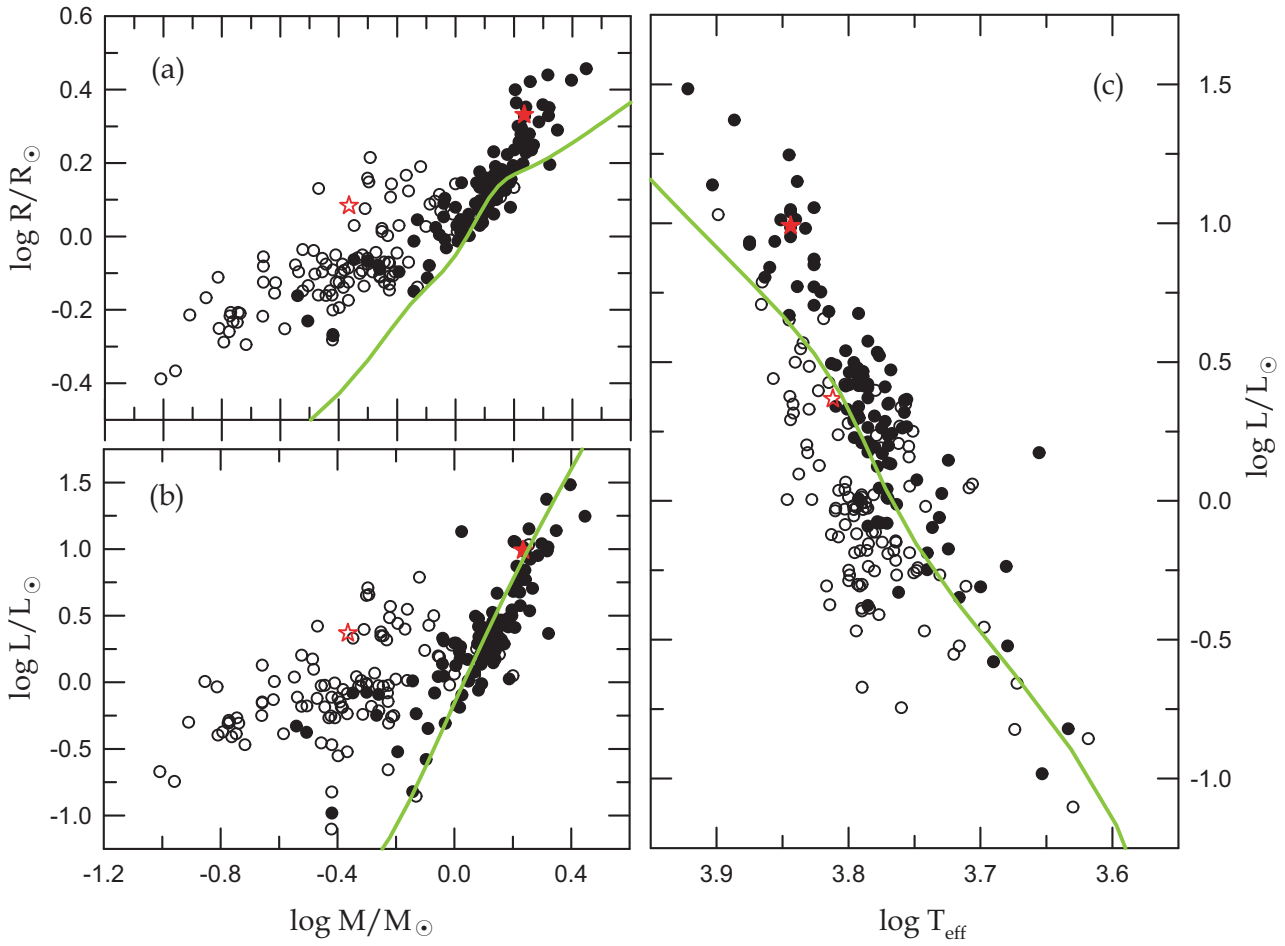

Fig. 5.— Plots of (a) mass-radius, (b) mass-luminosity, and (c) HR diagrams for W UMa-type eclipsing systems. The filled and open circles represent the more massive and less massive components, respectively. The star symbols denote the locations of the components of V407 Peg in these diagrams. The solid lines correspond to the zero-age main sequence stars calculated as having a solar metallicity of Z=0.02 by Tout et al. (1996).

Table 1. CCD photometric observations of V407 Peg.

HJD	ΔB	HJD	ΔV	HJD	$\Delta R_{\rm C}$
2,455,826.06512	−2.3954	2,455,826.06669	−2.2111	2,455,826.06751	−2.0998
2,455,826.06896	−2.4170	2,455,826.06942	−2.2368	2,455,826.06794	−2.1066
2,455,826.07045	−2.4292	2,455,826.09630	−2.3818	2,455,826.06826	−2.1152
2,455,826.07079	−2.4268	2,455,826.09763	−2.3923	2,455,826.06977	−2.1183
2,455,826.07121	−2.4312	2,455,826.09959	−2.3939	2,455,826.09666	−2.2579
2,455,826.07157	−2.4383	2,455,826.10086	−2.4051	2,455,826.09814	−2.2544
2,455,826.07192	−2.4703	2,455,826.10224	−2.4118	2,455,826.09857	−2.2703
2,455,826.07888	−2.4889	2,455,826.10352	−2.4134	2,455,826.09995	−2.2629
2,455,826.07922	−2.4898	2,455,826.10471	−2.4174	2,455,826.10123	−2.2749
2,455,826.08321	−2.5064	2,455,826.10596	−2.4188	2,455,826.10382	−2.2875

Note. — This table is available in its entirety in machine-readable and Virtual Observatory (VO) forms in the online journal. A portion is shown here for guidance regarding its form and content.

Table 2. Radial velocity and light-curve sets for V407 Peg.

Reference	Season	Data type	σ
Rucinski et al. (2008)	2006−2007	RV1	5.5 km s^{-1}
		RV2	15.2 km s^{-1}
SOAO	2011	B	0.011 mag
		V	0.010 mag
		$R_{\rm C}$	0.010 mag

Table 3. RV and light curve parameters of V407 Peg.

Parameter	Model 1		Model 2	
	Primary	Secondary	Primary	Secondary
T_0 (HJD)	2,452,534.6105(29)		2,452,534.6100(28)	
P (day)	0.63688436(57)		0.63688436(53)	
γ (km s^{-1})	7.9(7)		7.9(7)	
a ($R_\odot$)	4.02(3)		4.02(3)	
q	0.251(3)		0.251(3)	
i (deg)	87.6(6)		87.6(5)	
T (K)	6980	6535(6)	6980	6484(5)
Ω	2.275(2)	2.275	2.261(3)	2.261
$\Omega_{\rm in}$	2.356		2.356	
f (%)	51		61	
X, Y	0.639, 0.254	0.638, 0.242	0.639, 0.254	0.638, 0.241
x_B, y_B	0.790, 0.275	0.804, 0.233	0.790, 0.275	0.806, 0.228
x_V, y_V	0.691, 0.289	0.708, 0.275	0.691, 0.289	0.711, 0.274
$x_{R_{\rm C}}$, $y_{R_{\rm C}}$	0.594, 0.293	0.614, 0.285	0.594, 0.293	0.617, 0.284
$l/(l_1+l_2+l_3)_B$	0.700(3)	0.149	0.716(4)	0.147
$l/(l_1+l_2+l_3)_V$	0.712(3)	0.164	0.717(4)	0.162
$l/(l_1+l_2+l_3)_{R_{\rm C}}$	0.719(3)	0.176	0.718(4)	0.173
l_{3B}[a]	0.151(3)		0.137(4)	
l_{3V}[a]	0.124(3)		0.121(4)	
$l_{3R_{\rm C}}$[a]	0.105(3)		0.109(4)	
r (pole)	0.4880(4)	0.2689(10)	0.4913(7)	0.2727(15)
r (side)	0.5332(7)	0.2830(13)	0.5381(10)	0.2877(19)
r (back)	0.5637(9)	0.3379(33)	0.5700(14)	0.3492(53)
r (volume)[b]	0.5295	0.2967	0.5344	0.3023
Spot parameters:				
Colatitude (deg)	88.0(2)	...	...	86.0(4)
Longitude (deg)	301.1(2)	...	...	130.9(2)
Radius (deg)	21.4(1)	...	...	47.3(2)
$T_{\rm spot}/T_{\rm local}$	1.109(1)	...	...	1.131(1)
$\Sigma W(O-C)^2$	0.0106		0.0104	

[a]Value at 0.75 phase.

[b]Mean volume radius.

Table 4. Spot and luminosity parameters for historical light curves.

Parameter	MKN	ASAS
T_0 (HJD)[a]	2,552.44592(70)	3,889.90252(28)
P (day)	0.636882(20)	0.63688428(24)
Colatitude$_2$ (deg)	85.6(7.4)	85.1(4.1)
Longitude$_2$ (deg)	146.4(3.4)	140.0(1.5)
Radius$_2$ (deg)	49.1(3.1)	45.6(8)
$T_{\rm spot,2}/T_{\rm local,2}$	1.131(6)	1.115(3)
$l_1/(l_1+l_2+l_3)_B$	0.696(45)	...
$l_1/(l_1+l_2+l_3)_V$	0.713(40)	0.718(30)
l_{3B}[b]	0.161(42)	...
l_{3V}[b]	0.126(37)	0.119(20)

[a]HJD 2,450,000 is suppressed.

[b]Value at 0.75 phase.

Table 5. New minimum timings of V407 Peg.

KvW[a]	WD[a]	Difference[b]	Filter	Min	References
2,552.4416±0.0011	2,552.4456±0.0014	−0.0040	V	I	MKN
2,582.3735±0.0020	2,582.3763±0.0015	−0.0028	BV	I	MKN
5,829.20831±0.00035	5,829.21299±0.00012	−0.00468	$BVR_{\rm C}$	I	This paper
5,830.16850±0.00027	5,830.16796±0.00013	+0.00054	$BVR_{\rm C}$	II	This paper
5,853.09626±0.00019	5,853.09605±0.00013	+0.00021	$BVR_{\rm C}$	II	This paper
5,860.10220±0.00016	5,860.10119±0.00008	+0.00101	$BVR_{\rm C}$	II	This paper

[a]HJD 2,450,000 is suppressed.

[b]Differences between columns (1) and (2).

Table 6. Physical properties of V407 Peg.

Parameter	Deb & Singh (2011)		This Work	
	Primary	Secondary	Primary	Secondary
a ($R_\odot$)	4.182±0.027		4.019±0.029	
q	0.256±0.006		0.2515±0.0032	
i (°)	71.11±0.67		87.55±0.54	
T (K)	7300±184	6438±141	6980±200	6484±200
Ω	2.240±0.009	2.240	2.2611±0.0026	2.2611
r	0.470±0.003	0.312±0.003	0.5344±0.0010	0.3023±0.0025
M ($M_\odot$)	1.922±0.023	0.492±0.015	1.718±0.026	0.432±0.009
R ($R_\odot$)	1.965±0.018	1.305±0.015	2.146±0.015	1.214±0.013
log g (cgs)	...	...	4.010±0.009	3.905±0.013
ρ (g cm^3)	...	...	0.245±0.006	0.341±0.013
L ($L_\odot$)	9.83±1.17	2.62±0.29	9.80±1.13	2.33±0.29
$M_{\rm bol}$ (mag)	...	...	+2.25±0.13	+3.81±0.14
BC (mag)	...	...	+0.03±0.01	+0.01±0.01
$M_{\rm V}$ (mag)	...	...	+2.22±0.13	+3.80±0.14
Distance (pc)	...	...	280±21	